Mechanics of Graphene Bubbles

Peng Wang, Wei Gao, Kaimin Yue, Zhiyi Cao, Kenneth M. Liechti, Rui Huang*

Department of Aerospace Engineering and Engineering Mechanics, University of Texas, Austin, TX 78712, USA
* Corresponding author: ruihuang@mail.utexas.edu

Abstract Pressurized graphene bubbles have been observed in experiments, which can be used to determine the mechanical and adhesive properties of graphene. A nonlinear plate theory is adapted to describe the deformation of a graphene monolayer subject to lateral loads, where the bending moduli of monolayer graphene are independent of the in-plane Young's modulus and Poisson's ratio. A numerical method is developed to solve the nonlinear equations for circular graphene bubbles, and the results are compared to approximate solutions by analytical methods based on membrane and linear plate theories. The adhesion energy of mechanically exfoliated graphene on silicon oxide is extracted from two reported data sets. The strain distribution of the graphene bubbles and transport of gas molecules among the bubbles are discussed. Moreover, the effect of van der Waals interactions between graphene and its underlying substrate is analyzed, including large-scale interaction for nanoscale graphene bubbles subject to relatively low pressures.

Keywords Graphene, Adhesion, van der Waals interactions

1. Introduction

Graphene bubbles have been observed in experiments. Stolyarova et al. [1] observed nanoscale bubbles when mechanically exfoliated graphene flakes were placed on top of a silicon substrate covered with a thermally grown silicon oxide layer and exposed to proton irradiation. Much larger graphene bubbles were observed when the graphene flakes were exposed to vapors of hydrofluoric acid (HF) and water. In both cases, gas was released from the silicon oxide and trapped underneath the impermeable graphene, resulting in formation of the bubbles. More recently, Georgiou et al. [2] reported that bubbles are regularly found at the silicon oxide/graphene interface in large flakes obtained by mechanical cleavage. They observed graphene bubbles with diameters ranging from tens of nanometers to tens of microns and a variety of shapes (circular, triangular, and diamond). Bubbles have also been observed in graphene grown on metals such as Pt (111) [3] and Ru (0001) [4]. While the origin of graphene bubbles has not been fully understood and may depend on the material systems and experimental conditions, several potential applications of the graphene bubbles have emerged. Using highly strained graphene nanobubbles, Levy et al. [3] demonstrated enormous pseudo-magnetic fields and suggested strain engineering as a viable means of mechanical control over electronic structure of graphene. Georgiou et al. [2] demonstrated controllable curvature of graphene bubbles by applying an external electric field, which may be used as optical lenses with variable focal length. Zabel et al. [5] used graphene bubbles to study the Raman spectrum of graphene under biaxial strain. A well-controlled pressurization method was developed by Bunch et al. [6] to form graphene bubbles (or balloons) on patterned substrates, which was used to demonstrate the impermeability of graphene to gas molecules and to measure elastic properties of graphene. Following a similar approach, Koenig et al. [7] measured the adhesion energy between graphene and silicon oxide. On the other hand, Zong et al. [8] used intercalation of nanoparticles to generate graphene blisters on silicon surface and thereby provided a measurement of the graphene adhesion.

The present study focuses on the mechanics of graphene bubbles in order to establish a theoretical relationship between the morphology of graphene bubbles and the mechanical as well as interfacial properties of graphene. We present a nonlinear plate theory, adapted for the in-plane and bending properties of monolayer graphene. A numerical method is developed to solve the nonlinear

equations for circular graphene bubbles, subjected to gas pressure and van der Waals interactions. The numerical results are compared to the approximate solutions obtained by analytical methods. We show that, with known elastic properties of graphene, the adhesion energy between graphene and its substrate can be determined from the measurable dimensions of a graphene bubble (e.g., diameter and height). We confirm that the strain of graphene is non-uniform, varying from an equibiaxial strain at the center of the bubble to a uniaxial strain at the edge. The magnitude of the strain depends on the adhesion energy. The mechanics of graphene bubbles is extended to discuss transport of gas molecules among graphene bubbles of different sizes and the coalescence of graphene bubbles from a thermodynamics perspective.

2. A Nonlinear Plate Theory for Monolayer Graphene

The mechanical behavior of a graphene monolayer can be described by a mixed continuum mechanics formulation mapping a two-dimensional (2D) plane to a three-dimensional (3D) space [9]. Under the assumption of relatively small deformation but with moderately large deflection, a set of nonlinear equations can be used, which closely resemble the von Karman equations for an isotropic elastic thin plate. The only notable difference lies in the bending moduli of graphene. Unlike classical plate theory, the bending moduli of monolayer graphene are not directly related to the in-plane Young's modulus and Poisson's ratio. Instead, they are determined from atomistic modeling as independent properties [10-14]. As discussed in a previous study [13], the physical origin of the bending moduli of the monolayer graphene is fundamentally different from those in classical plate theory. In particular, we note that it is unnecessary to define a thickness for the graphene monolayer in the 2D continuum formulation.

Consider a circular graphene membrane subjected to axisymmetric loading. The displacements expressed in polar coordinates are: $u_r = u(r)$, $u_\theta = 0$, and $w = w(r)$. The corresponding in-plane strain components are:

$$\varepsilon_r = \frac{du}{dr} + \frac{1}{2}\left(\frac{dw}{dr}\right)^2, \tag{1}$$

$$\varepsilon_\theta = \frac{u}{r}. \tag{2}$$

The radial and circumferential membrane forces are

$$N_r = \frac{E_{2D}}{1-\nu^2}\left(\frac{du}{dr} + \nu\frac{u}{r} + \frac{1}{2}\left(\frac{dw}{dr}\right)^2\right), \tag{3}$$

$$N_\theta = \frac{E_{2D}}{1-\nu^2}\left(\nu\frac{du}{dr} + \frac{u}{r} + \frac{\nu}{2}\left(\frac{dw}{dr}\right)^2\right), \tag{4}$$

where E_{2D} is the 2D Young's modulus of graphene and ν is Poisson's ratio. The in-plane force equilibrium equation reduces to a nonlinear displacement equation

$$\frac{d^2u}{dr^2} + \frac{1}{r}\frac{du}{dr} - \frac{u}{r^2} = -\frac{1-\nu}{2r}\left(\frac{dw}{dr}\right)^2 - \frac{dw}{dr}\frac{d^2w}{dr^2}. \tag{5}$$

The bending moments are:

$$M_r = D\frac{d^2w}{dr^2} + \left(D - D_G\right)\frac{1}{r}\frac{dw}{dr}, \tag{6}$$

$$M_\theta = (D - D_G)\frac{d^2w}{dr^2} + \frac{D}{r}\frac{dw}{dr}, \tag{7}$$

where D and D_G are the two bending moduli corresponding to the mean curvature and the Gaussian curvature, respectively. The moment equilibrium equation leads to another nonlinear displacement equation

$$D\left(\frac{d^3w}{dr^3} + \frac{1}{r}\frac{d^2w}{dr^2} - \frac{1}{r^2}\frac{dw}{dr}\right) - \frac{E_{2D}}{1-\nu^2}\frac{dw}{dr}\left(\frac{du}{dr} + \nu\frac{u}{r} + \frac{1}{2}\left(\frac{dw}{dr}\right)^2\right) = \frac{1}{r}\int_0^r qrdr, \tag{8}$$

where q is the lateral loading intensity (e.g., pressure). In the present study, the lateral load intensity consists of a constant pressure (p) and the van der Waals (vdW) force between graphene and the substrate, i.e., $q = p - \sigma_{vdW}$, where $\sigma_{vdW} > 0$ for attractive force. By a simple model of vdW interactions [15], the vdW force is written as a function of deflection:

$$\sigma_{vdW}(w) = \frac{9\Gamma}{2\delta_0}\left[\left(\frac{\delta_0}{w+\delta_0}\right)^4 - \left(\frac{\delta_0}{w+\delta_0}\right)^{10}\right], \tag{9}$$

where δ_0 is the equilibrium separation and Γ is the interfacial adhesion energy. For monolayer graphene on SiO_2, experimental measurements have reported values from 0.4 to 0.9 nm for δ_0 [16-18] and from 0.09 to 0.45 J/m^2 for Γ [7, 8]. In the present study, we take $\delta_0 = 0.6$ nm and $\Gamma = 0.1$ J/m^2. For monolayer graphene bubbles, we use E_{2D} = 345 N/m, ν = 0.16, and D = 1.5 eV (or equivalently, 0.238 nN-nm). The radii of the graphene bubbles ranges from 10 to 1000 nm, and n = 1000 is used for the finite difference discretization.

3. Analytical Methods

Several approximate solutions for graphene bubbles were presented in a previous study [19]. They are briefly reviewed here for comparison with the numerical results.

3.1. Linear plate solution

For the linear plate analysis, the in-plane strain is assumed to be negligible, and Eq. (8) reduces to

$$D\left(\frac{d^3w}{dr^3} + \frac{1}{r}\frac{d^2w}{dr^2} - \frac{1}{r^2}\frac{dw}{dr}\right) = \frac{1}{r}\int_0^r qrdr. \tag{10}$$

Subjected to a uniform lateral load ($q = p$) and clamped boundary condition at the edge (i.e., $w = dw/dr = 0$ at $r = a$), Eq. (10) can be solved analytically by

$$w = h\left(1 - \frac{r^2}{a^2}\right)^2, \tag{11}$$

where a is the bubble radius and $h = \frac{pa^4}{64D}$ is the center deflection (bubble height).

3.2. An approximate membrane solution

For a membrane analysis, it is assumed that the bending stiffness is negligible. The nonlinear membrane equations however cannot be solved analytically. An approximate solution was developed by the energy method assuming the displacements [19]:

$$w = h\left(1 - \frac{r^2}{a^2}\right), \tag{12}$$

$$u = u_0 \frac{r}{a}\left(1 - \frac{r}{a}\right), \tag{13}$$

where $h = \left[\phi(\nu) pa^4 / E_{2D}\right]^{1/3}$ and $u_0 = \left[\psi(\nu) p^2 a^5 / E_{2D}^2\right]^{1/3}$, with $\phi(\nu) = \frac{75(1-\nu^2)}{8(23+18\nu-3\nu^2)}$ and $\psi(\nu) = \frac{45(3-\nu)^3(1-\nu^2)^2}{8(23+18\nu-3\nu^2)^2}$. A more accurate membrane analysis was developed by Hencky [20], which included 7 terms in the polynomial expansion of the deflection profile (as opposed to the two terms in Eq. 12) with the coefficients determined numerically for specific Poisson's ratios. In particular, for $\nu = 0.16$, the center deflection by Hencky's solution is: $h = 0.687\left(pa^4 / E_{2D}\right)^{1/3}$.

3.3. An approximate nonlinear plate solution

An energy method was used to develop an approximate solution to the nonlinear plate equations by assuming a deflection profile in form of (11) along with the radial displacement [19]

$$u = r(a-r)(c_1 + c_2 r). \tag{14}$$

Minimization of the potential energy leads to

$$c_1 = \frac{179 - 89\nu}{126}\frac{h^2}{a^3}, \tag{15}$$

$$c_2 = \frac{13\nu - 79}{42}\frac{h^2}{a^4}, \tag{16}$$

$$p = 64\eta(\nu)\frac{E_{2D}h^3}{a^4} + 64\frac{Dh}{a^4}, \tag{17}$$

where $\eta(\nu) = \frac{7505 + 4250\nu - 2791\nu^2}{211680(1-\nu^2)}$. It was shown that the approximate solution converges to the linear plate solution when the bubble height is small (h < 0.1 nm) but considerably underestimates the pressure when h > 1 nm.

4. A Numerical Method

A numerical method is developed to solve the coupled nonlinear equations, (5) and (8). For convenience we define an effective thickness, $h_e = \sqrt{\frac{12(1-\nu^2)D}{E_{2D}}}$, and re-write the equations in a dimensionless form

$$g = \frac{d^2\bar{u}}{d\bar{r}^2} + \frac{1}{\bar{r}}\frac{d\bar{u}}{d\bar{r}} - \frac{\bar{u}}{\bar{r}^2} + \frac{1-\nu}{2\bar{r}}\theta^2 + \theta\frac{d\theta}{d\bar{r}} = 0, \tag{18}$$

$$f = \frac{d^2\theta}{d\bar{r}^2} + \frac{1}{\bar{r}}\frac{d\theta}{d\bar{r}} - \frac{\theta}{\bar{r}^2} - 12\theta\left(\frac{d\bar{u}}{d\bar{r}} + \nu\frac{\bar{u}}{\bar{r}} + \frac{\theta^2}{2}\right) - \frac{1}{\bar{r}}\int_0^{\bar{r}} \bar{q}\bar{r}d\bar{r} = 0, \tag{19}$$

where $\theta = \frac{dw}{dr}$, $\bar{r} = \frac{r}{h_e}$, $\bar{u} = \frac{u}{h_e}$ and $\bar{q} = \frac{qh_e^3}{D}$. The equations are discretized by the finite difference method and solved by the Newton-Raphson method. At each iteration, the residuals are calculated and a correction vector is calculated as

$$\begin{pmatrix} \Delta\boldsymbol{\theta} \\ \Delta\bar{\mathbf{u}} \end{pmatrix} = -\begin{bmatrix} \dfrac{\partial \mathbf{f}}{\partial \boldsymbol{\theta}} & \dfrac{\partial \mathbf{f}}{\partial \bar{\mathbf{u}}} \\ \dfrac{\partial \mathbf{g}}{\partial \boldsymbol{\theta}} & \dfrac{\partial \mathbf{g}}{\partial \bar{\mathbf{u}}} \end{bmatrix}^{-1} \begin{pmatrix} \mathbf{f} \\ \mathbf{g} \end{pmatrix}, \tag{20}$$

where $\Delta\boldsymbol{\theta}$ is a vector of n-1 components ($\Delta\theta_k$, k = 1 to n-1) and same for $\Delta\mathbf{u}$, $\mathbf{f}$, and $\mathbf{g}$. The Jacobian matrix on the right-hand side of (20) consists of four square blocks, each with a rank of n-1. For the convergence criterion, we require that the L2-norm of the relative correction vector is smaller than a specified tolerance, namely

$$|\mathbf{R}| = \left[\sum_{k=1}^{n-1}\left(\Delta\theta_k^2/\theta_k^2 + \Delta u_k^2/u_k^2\right)\right]^{1/2} < \tau \sim 10^{-4}. \tag{21}$$

If not satisfied, the iteration procedure repeats with a new approximation, $\theta_k^{(i+1)} = \theta_k^{(i)} + \Delta\theta_k$ and $\bar{u}_k^{(i+1)} = \bar{u}_k^{(i)} + \Delta u_k$. Once converged, we calculate the deflection at each node by numerical integration:

$$\bar{w}_k = -\frac{\bar{a}}{2n}\sum_{m=k}^{n-1}\left(\theta_m + \theta_{m+1}\right). \tag{22}$$

for k = 0 to n-1, and the center deflection is then obtained as $h = w_0$. Moreover, we calculate the strain components at each node according to (1) and (2).

5. Results and Discussions

Using the numerical method in Section 4, we calculated the deflection profiles, $w(r)$, for graphene bubbles of various radii. Figure 1(a) shows the normalized deflection for a graphene bubble of radius a = 10 nm subject to increasing pressure (without van der Waals interaction). The deflection is normalized by the center deflection, $h = w_0$. In comparison, the analytical deflection profiles in (11) and (12) from the linear plate solution and the approximate membrane analysis are both independent of the pressure after the normalization. The numerical result agrees well with the linear plate solution at low pressures. As the pressure increases, the deflection profile approaches the membrane solution. Apparently, (12) is a reasonably good approximation for the deflection profile at high pressures. A more accurate membrane analysis [20] would yield a better approximation but also require a numerical method. Therefore, the analytical solutions in (11) and (12) may be considered as the lower and upper bounds for the deflection profiles.

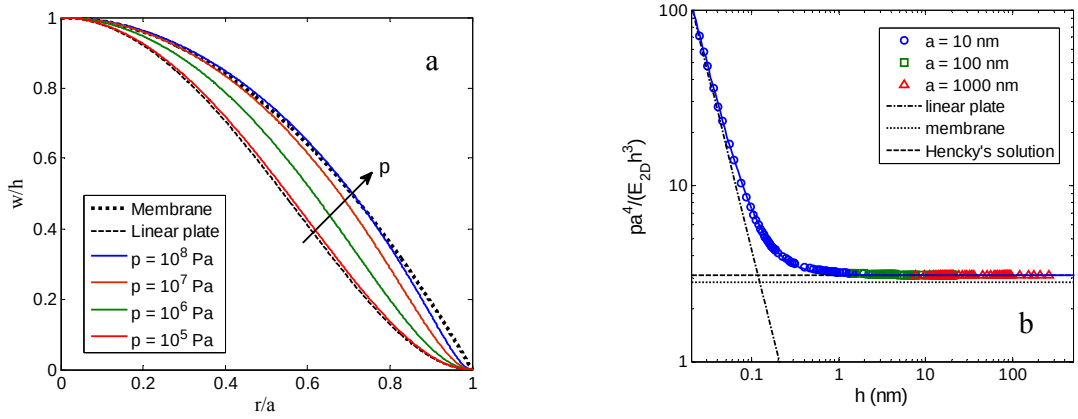

Figure 1. (a) Normalized deflection profiles of a graphene bubble (a = 10 nm) subject to increasing pressure; (b) Normalized pressure as a function of the center deflection.

The center deflection of a graphene bubble is a function of the pressure and the bubble radius. The linear plate solution predicts that the center deflection increases linearly with pressure ($h \propto p$). On the other hand, from the membrane analysis, the cube of the center deflection increases linearly with pressure ($h^3 \propto p$). We plot the center deflection versus a dimensionless group, $pa^4/(E_{2D}h^3)$, as shown in Fig. 1(b). In such a plot, the numerical results for different bubble radii collapse onto one master curve. When h > 1 nm, the numerical results agree closely with Hencky's membrane solution, while the simple membrane analysis in Section 3.2 underestimates the normalized pressure. It is found that the numerical results can be fitted by a single function that is a simple sum of the linear plate solution and the membrane solution:

$$\frac{pa^4}{E_{2D}h^3} = A(\nu) + B(\nu)\left(\frac{h_e}{h}\right)^2, \tag{23}$$

where A and B are two dimensionless functions of Poisson's ratio. From the membrane solution, $A = 1/\phi(\nu)$, which equals 2.825 for $\nu = 0.16$. On the other hand, Hencky's solution yields $A = 3.09$ for $\nu = 0.16$. From the linear plate solution, $B = \dfrac{16}{3(1-\nu^2)}$. The effective thickness, $h_e = \sqrt{\dfrac{12(1-\nu^2)D}{E_{2D}}}$, defines a length scale for the monolayer graphene. Therefore, the transition from the linear plate solution to the membrane solution depends on the ratio h/h_e. For relatively large bubbles (e.g., a > 100 nm), since the center deflection is typically much greater than h_e, the second term on the right-hand side of (23) is negligible and Hencky's membrane solution is sufficient.

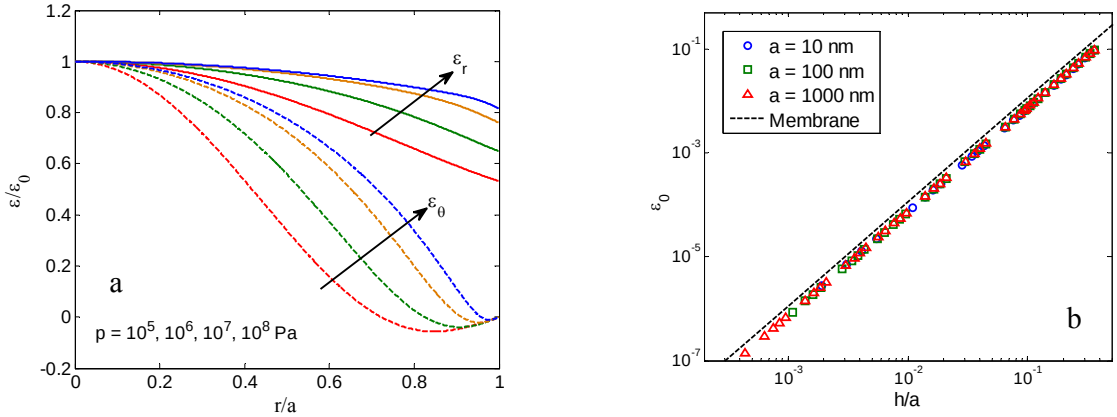

Figure 2. (a) Strain distributions in graphene bubbles (a = 10 nm) subject to increasing pressure; (b) Center strain versus h/a.

The strain distribution is important for strain engineering as a potential approach to manipulating the electronic properties of graphene [3, 4]. Figure 2(a) shows the strain distribution in graphene bubbles. By the symmetry and boundary conditions, the strain is equi-biaxial at the center (r = 0) and uniaxial at the edge ($r = a$). However, the strain distribution in between is very different from the prediction by the simple membrane analysis in Section 3.2. By inserting (12) and (13) into (1) and (2), the circumferential strain ε_θ would decrease linearly from the center to the edge, while the radial strain ε_r first decreases and then increases [19]. Moreover, the analytical membrane solution predicts that the normalized strain distribution should be independent of the pressure or the bubble radius. However, the numerical results clearly demonstrate that the strain distribution (after normalization) depends on both the pressure and the bubble radius. The difference in the strain

distribution between the numerical and the analytical solutions can be traced back to the difference in the deflection profiles as shown in Fig. 1(a). Furthermore, the in-plane radial displacement obtained by the numerical method differs from the analytical assumption in (13). Notably, the radial displacement becomes negative near the edge, resulting in compressive circumferential strain ($\varepsilon_\theta < 0$).

The equi-biaxial strain at the center ($\varepsilon_r = \varepsilon_\theta = \varepsilon_0$) is plotted in Figure 3(b) as a function of the normalized pressure. Noting that the center strain $\varepsilon_0 \propto (h/a)^2$ in both analytical solutions, we plot the numerical results as a function of *h*/*a* in Fig. 2(b). Indeed the numerical results for different bubble radii collapse onto one line with the slope 2 in the log-log plot. Therefore, the center strain may be written as

$$\varepsilon_0 = C(\nu)\left(\frac{h}{a}\right)^2, \tag{24}$$

where $C(\nu)$ is a dimensionless functions of Poisson's ratio. By the membrane solution in Section 3.2, $C(\nu) = \psi^{1/3}/\phi^{2/3}$, which equals 1.136 for $\nu = 0.16$. The numerical results can be fitted approximately by taking $C(\nu) = 0.76$. Therefore, the analytical membrane solution overestimates the center strain considerably.

Based on the membrane analysis, the adhesion energy of between graphene and its substrate can be determined from the measurements of the equilibrium bubble size (*a* and *h*) [19]. With the number of gas molecules (*N*) fixed inside the bubble, the potential energy is obtained as a function of the bubble radius

$$\Pi(a, N) = \frac{Nk_BT}{4} - Nk_BT \ln\left[\frac{p_0 a^{5/2}}{(Nk_BT)^{3/4} E_{2D}^{1/4}}\right], \tag{25}$$

where p_0 is the ambient pressure outside the bubble and k_B is Boltzmann constant. The first term on the right hand side of (25) is the strain energy in graphene, which is independent of the bubble size under the condition of constant *N*. The second term is the potential energy of the gas, relative to the reference state in the ambient condition. As the bubble radius *a* increases, the total potential energy decreases. Meanwhile, the interfacial energy increases as part of the graphene is detached from the substrate. The equilibrium bubble radius is attained when the potential energy of the bubble is balanced by the adhesion energy (Γ) of the graphene/substrate interface, which gives rise to the adhesion energy

$$\Gamma = -\frac{1}{2\pi a}\left(\frac{\partial \Pi}{\partial a}\right)_N = \frac{5Nk_BT}{4\pi a^2} = \frac{5E_{2D}h^4}{8\phi a^4}. \tag{26}$$

Combining (24) and (26), we have $\varepsilon_0 \propto (\Gamma / E_{2D})^{1/2}$. Therefore, the magnitude of the strain depends on the adhesion energy. This suggests that strain measurement could be used as an alternate approach for determining the adhesion energy [19]. On the other hand, to achieve a relatively large strain (> 5%) for strain engineering to manipulate the electronic properties of graphene [3, 4], the adhesion energy must be sufficiently high.

Georgiou et al. [2] measured the cross-sectional profile of a graphene bubble on an oxidized silicon substrate by atomic force microscope (AFM) in tapping mode. The bubble radius and central deflection were determined as $a = 1183$ nm and $h = 132$ nm. Using these values in (26), we obtain the adhesion energy Γ = 0.097 J/m^2. The data set from Koenig et al. [7] puts the adhesion energy in the range between 0.25 and 0.43 J/m^2, with an average value of 0.33 J/m^2. These values

are lower than the reported value (0.45 J/m^2) for monolayer graphene on silicon oxide [7]. The difference is partly attributed to the approximations made in the present membrane analysis as opposed to Hencky's solution used by Koenig et al. [7]. The scattering of the adhesion energy from these data suggest that the adhesion energy could be non-uniform due to the statistical nature of the surface roughness [21].

Stolyarova et al. [1] observed coalescence of graphene bubbles during annealing, which can be understood as a result of the transport of gas molecules along the interface driven by the different pressures in bubbles of different sizes. The membrane analysis predicts that the pressure inside the graphene bubble is inversely proportional to the bubble radius [19]. Consequently, the pressure is higher in the smaller bubbles and the pressure difference drives the gas molecules to diffuse from smaller bubbles to larger bubbles. The diffusion process is kinetically mediated and is enhanced by thermal annealing so that the large bubbles grow larger while the small bubbles disappear, similar to the Ostwald ripening process in thin film growth. The coalescence of graphene bubbles may also be understood from an energy consideration. It can be shown that the free energy of two small bubbles is greater than the free energy of one large bubble with the same total number of gas molecules [19]. Therefore, there exists a thermodynamic driving force for the two small bubbles to coalesce so that the total free energy is reduced. In other words, while each graphene bubble is in a thermodynamically equilibrium state, the system with a group of graphene bubbles is not in equilibrium. Since the graphene is impermeable [6], the kinetic pathways for the transport of gas molecules may include the graphene/substrate interface and the substrate bulk.

Figure 3(a) shows the deflection profiles of a graphene bubble (a = 10 nm) under the effect of vdW interaction. When the pressure is relatively low, the deflection is reduced considerably by the attractive vdW force. On the other hand, when the pressure is high, the effect of vdW force on the deflection is negligible. As shown in Fig. 3(b), the distribution of vdW force is non-uniform and depends on the pressure. In the spirit of nonlinear fracture mechanics [22], we may define an interaction zone where the vdW force is appreciable in comparison with the pressure, e.g., $\sigma_{vdW} > p/10$. Subject to a low pressure, the interaction zone spans the entire area underneath the bubble, indicating large-scale bridging from a fracture mechanics perspective. At a higher pressure level, the interaction zone is much smaller, where the condition of small-scale bridging prevails. Consequently, in the presence of vdW interactions, the relationship between the center deflection and the pressure becomes nonlinear at low pressures.

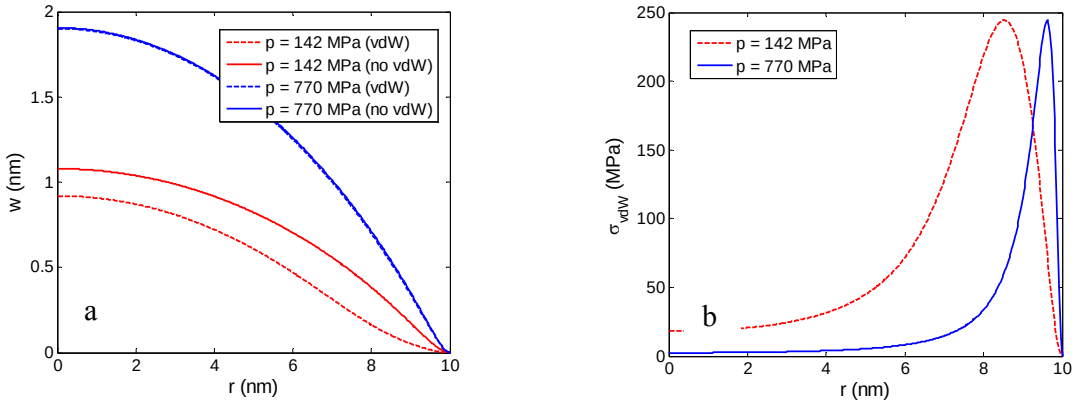

Figure 3. (a) Effect of the vdW interaction on the deflection profile of a graphene bubble (a = 10 nm); (b) Distributions of the vdW force intensity.

6. Summary

A nonlinear plate theory is adapted to describe the deformation of a graphene monolayer subject to lateral loads. A numerical method is developed to solve the nonlinear equations for circular graphene bubbles. In comparison to approximate solutions by analytical methods, it is found that the deflection profile and the strain distribution are generally not well described by the analytical solutions. Based on the numerical results, approximate formulae for the center deflection and center strain are suggested. We show that, with known elastic properties of graphene, the adhesion energy between graphene and its substrate can be determined from the measurable dimensions of a graphene bubble (e.g., diameter and height). The mechanics of graphene bubbles is extended to discuss transport of gas molecules among graphene bubbles of different sizes and the coalescence of graphene bubbles from a thermodynamics perspective. Moreover, the effect of van der Waals interactions between graphene and its substrate is found to be significant when the center deflection is relatively small due to large-scale adhesive interactions.

Acknowledgements

The authors gratefully acknowledge financial support of this work by the National Science Foundation through Grant Nos. CMMI-0926851 and CMMI-1130261.

References

1. Stolyarova, E., et al., 2009, "Observation of graphene bubbles and effective mass transport under graphene films", Nano Lett. 9, 332-337.
2. Georgiou, T., et al., 2011, "Graphene bubbles with controllable curvature," Appl. Phys. Lett. 99, 093103.
3. Levy, N., et al., 2010, "Strain-induced pseudo-magnetic fields greater than 300 Tesla in graphene nanobubbles," Science 329, 544-547.
4. Lu, J., Castro Neto, A.H., Loh, K.P., 2012, "Transforming moire blisters into geometric graphene nano-bubbles," Nature Communications 3: 823.
5. Zabel, J., et al., 2012, "Raman spectroscopy of graphene and bilayer under biaxial strain: bubbles and balloons" Nano Lett. 12, 617-621.
6. Bunch, J. S., et al., 2008, "Impermeable atomic membranes from graphene sheets," Nano Lett. 8, 2458-2462.
7. Koenig, S. P., Boddeti, N. G., Dunn, M. L., Bunch, J. S., 2011, "Ultrastrong adhesion of graphene membranes," Nature Nanotechnology 6, 543-546.
8. Zong, Z., Chen, C.-L., Dokmeci, M. R., Wan, K.-T., 2010, "Direct measurement of graphene adhesion on silicon surface by intercalation of nanoparticles," J. Appl. Phys. **107**, 026104.
9. Lu, Q. and Huang, R., 2009, "Nonlinear mechanics of single-atomic-layer graphene sheets," Int. J. Applied Mechanics **1**, 443-467.
10. Kudin, K. N., Scuseria, G. E., and Yakobson, B. I., 2001, "C_2F, BN, and C nanoshell elasticity from ab initio computations," Phys. Rev. B, **64**, 235406.
11. Arroyo, M., and Belytschko, T., 2004, "Finite crystal elasticity of carbon nanotubes based on the exponential Cauchy-Born rule," Phys. Rev. B, **69**, 115415.
12. Huang, Y., Wu, J., Hwang, K. C., 2006, "Thickness of graphene and single-wall carbon nanotubes," Phys. Rev. B, **74**, 245413.
13. Lu, Q., Arroyo, M., Huang, R., 2009, "Elastic bending modulus of monolayer graphene," J. Phys. D: Appl. Phys. **42**, 102002.
14. Koskinen, P., and Kit, O. O., 2010, "Approximate modeling of spherical membranes," Phys. Rev. B **82**, 235420 (2010).
15. Aitken, Z. H., and Huang, R., 2010, "Effects of mismatch strain and substrate surface corrugation on morphology of supported monolayer graphene," J. Appl. Phys. **107**, 123531.
16. Ishigami, M., Chen, J. H., Cullen, W. G., Fuhrer, M. S., Williams, E. D., 2007, "Atomic structure of graphene on SiO_2," Nano Lett. **7**, 1643-1648.
17. Gupta, A., Chen, G., Joshi, P., Tadigadapa, S., and Eklund, P. C., 2006, "Raman scattering from high-frequency phonons in supported n-graphene layer films" Nano Lett. **6**, 2667-2673.

18. Sonde, S., Giannazzo, F., Raineri, V., and Rimini, E., 2009, "Dielectric thickness dependence of capacitive behavior in graphene deposited on silicon dioxide," J. Vac. Sci. Technol. B **27**, 868-873.
19. Yue, K., Gao, W., Huang, R., Liechti, K.M., 2012, "Analytical methods for the mechanics of graphene bubbles," J. Appl. Phys., **112**, 083512.
20. Hencky, H., 1915, *Zeitschrift fur Mathematik und Physik* 63, 311–317.
21. Gao, W., and Huang, R., 2011, "Effect of surface roughness on adhesion of graphene membranes" J. Phys. D: Appl. Phys. **44**, 452001.
22. Hutchinson, J. W., and Evans, A. G., 2000, "Mechanics of materials: top-down approaches to fracture," Acta Materialia **48**, 125–135.